Optical Materials 154 (2024) 115785

Contents lists available at ScienceDirect

Optical Materials

journal homepage: www.elsevier.com/locate/optmat

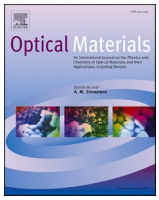

Research Article

The figure of merit improvement of (Sn, Co)–ZnO sprayed thin films for optoelectronic applications

Imadeddine Bellili [a,*], Mohamed Mahtali [a], Warda Darenfad [a], Noubeil Guermat [b,c]

[a] Thin Films and Interfaces Laboratory (LCMI), University of Constantine 1, 25000, Constantine, Algeria
[b] Department of Electronics, Faculty of Technology, University of M'sila, PO Box 166 Ichebilia, 28000, M'sila, Algeria
[c] Laboratoire des Etudes de Matériaux d'Electronique pour Applications Médicales (LEMEAMED), Université de Constantine 1, 25000, Constantine, Algeria

ARTICLE INFO

Keywords:
Undoped ZnO
(Sn, Co) co-doped ZnO
Pneumatic spray pyrolysis
Nanocrystalline
Figure of merit

ABSTRACT

Nanocrystalline zinc oxide (ZnO) has garnered significant attention from researchers and industries due to its superior properties as an optoelectronic material, particularly in solar cells as a transparent electrode. Doping, especially with tin (Sn) and co-doping with tin and cobalt (Co), can refine its optoelectronic properties. In this manuscript, we report on the optoelectronic properties of undoped ZnO thin films, as well as those doped with Sn and/or Co, elaborated using a simple chemical pneumatic spray pyrolysis method on glass substrates. A 1 % Sn doping concentration was used, with Co doping concentrations of 0 %, 0.5 %, and 1 %. The effects of Sn and/or Co doping concentration on the structure, morphology, optical, and electrical properties of nanocrystalline ZnO were studied using X-ray diffractometer (XRD), Raman spectroscopy, Field emission scanning electron microscopy (FESEM), UV–Vis–NIR spectroscopy and Hall effect measurements. All the films studied exhibit wurtzite ZnO structures with a predominant (002) orientation and no secondary phase, as confirmed by X-ray diffraction (XRD) analysis. The Raman spectroscopy also reveals the presence of a wurtzite structure in all the films. The FESEM images reveal the kind and concentration of the dopants significantly influenced the surface morphology of the films. The elemental analysis with energy dispersive X-ray analysis (EDS) analysis successfully detected the doping of Sn and Co. The analysis of UV–Vis spectroscopy provide that the optical band gap for the undoped ZnO film is 3.25 eV. This band gap increases upon doping and co-doping, reaching a peak value of 3.30 eV for the Sn: Co (1 %:0.5 %) co-doped ZnO film. The ZnO film shows an improvement in the electrical resistivity upon doping and co-doping with low resistivity value of 1.95×10^{-2} Ω cm for the film (1%Sn, 0.5 % Co)–ZnO. The highest figure of merit (FOM) achieved is 1.41×10^{-4} Ω^{-1} for a ZnO thin film co-doped with (1 % Sn, 0.5 % Co). The existence of (1 % Sn, 0.5 % Co) film with improved optical gap, low electrical resistivity and high FOM supports its use in transparent conductive oxide applications.

1. Introduction

Transparent conductive oxides (TCOs) are attracting considerable interest due to their potential for various applications such as microelectronics, optoelectronics [1], anti-corrosion [2], thermal mirrors [3], surface plasmon resonance sensor [4], etc. Among the best-known TCOs are the oxides of zinc (ZnO), cadmium (CdO), tin (SnO_2), indium (In_2O_3) and gallium (Ga_2O_3). In this study, we focus on ZnO due to its non-toxicity, low cost, high chemical and thermal stability, and its abundance in nature. Many attempts have been made to improve these properties by varying the stoichiometric ratio with the addition of dopants to the ZnO matrix [5], in order to increase their use as transparent electrodes in optoelectronic applications such as solar cells, laser diodes, light-emitting diodes and flat screens. So, the right choice and incorporation of suitable doping or co-doping with optimal concentrations in the ZnO matrix can improve the electrical conductivity or transmittance. For example, Guermat et al. [6] reported a high transmission of 93 % for the ZnO film doped with 3%Ni deposited by the spray pyrolysis technique. Darenfad et al. [7] prepared different films of pure ZnO, $Zn_{0.97}Mg_{0.03}O$, $Zn_{0.96}Mg_{0.03}Mn_{0.01}O$ and $Zn_{0.90}Mg_{0.03}Mn_{0.01}F_{0.06}O$, on plain glass substrates using spray pyrolysis technique. Their results showed that the $Zn_{0.90}Mg_{0.03}Mn_{0.01}F_{0.06}O$ film exhibited a minimum resistivity of approximately 1.33×10^{-3} Ω cm, while the $Zn_{0.97}Mg_{0.03}O$ film achieved a maximum optical transmission

* Corresponding author.
E-mail address: imadeddine.billili@doc.umc.edu.dz (I. Bellili).

https://doi.org/10.1016/j.optmat.2024.115785
Received 9 March 2024; Received in revised form 22 June 2024; Accepted 7 July 2024
Available online 7 July 2024

above 91 %. Conversely, the addition of impurities can negatively impact the optical and electrical properties of materials [8,9]. According to Darenfad et al. [10], the ZnO:6%F:1%Mg film deposited by spray pyrolysis has a high electrical conductivity, measured at 0.030 $(\Omega\,cm)^{-1}$. Tiwari et al. [11] showed that the co-doping of thin layers of ZnO with Sn–In, deposited by sol-gel, improves optical transmission and makes it possible to obtain an electrical resistivity of approximately 0.5 Ω cm. Recent studies on thin films of $Zn_{1-x}Sn_xO$ (x = 0.01 and 0.03) have shown that doping affects the optical properties, leading to a decrease in transmittance as the bandgap energy values increase from 3.254 eV to 3.258 eV [12]. Thus, to obtain effective transparent conductive oxides in optoelectronic applications, it is necessary to find a balance between optical transparency and electrical conductivity. This balance is the main object of our study. It is therefore crucial to identify the elements that can be added to ZnO to increase the bandgap, improve the electrical conductivity and increase the carrier concentration. In this study, the first choice of dopant is tin (Sn), due to its excellent properties such as high conductivity, non-toxicity, low cost and availability. In addition, the ionic radius of Sn^{+4} (0.069 nm) is smaller than that of Zn^{+2} (0.074 nm), which allows it to effectively substitute for Zn ions in the ZnO matrix [11]. Replacing zinc with tin results in a significant improvement in electrical conductivity by introducing two additional free electrons [13]. Furthermore, researchers, including the authors, have reported that optical transparency and electrical conductivity of ZnO films improve with Sn-doping [14]. Ganesh et al. [15] observed that the transmittance of ZnO:%Sn thin films deposited by spin coating technique is high for low concentrations of Sn (1 %, 3 %), but decreases at higher concentrations of Sn (5 %, 7 %). Therefore, these characteristics of Sn indicate that it is a promising candidate for use as an n-type dopant in ZnO. Furthermore, numerous studies on ZnO thin films have shown that the electrical properties can be significantly enhanced through the simultaneous incorporation of two or three different dopants [6,7]. In this context, the effect of Sn/Co co-doping on the opto-electronic properties of ZnO films had not been studied by researchers, which inspired the conduct of this study. For cobalt (Co) doping in the ZnO lattice, we have selected this dopant because, when exposed to light, the Co^{+2} cation becomes ionized, forming the Co^{+3} cation [6]. This ionization releases an electron that is incorporated into the conduction band, thereby enhancing the electrical conductivity of the films under light excitation [6]. Furthermore, the high solubility and significantly smaller ionic radius of Co^{+2} (0.058 nm) compared to Zn^{+2} make it well-suited for replacing Zn^{+2} ions [16]. Demirselcuk et al. [17] conducted a study on the synthesis and characterization of ZnO:Co thin films (0, 2, 4 and 6 at.%) deposited by spray pyrolysis, focusing on their optical transmittance and electrical resistivity. Their findings underscored the impact of cobalt doping on optical properties, revealing an increase in electrical resistivity with higher Co concentrations. In contrast, Guermat et al. [6] investigated undoped and co-doped ZnO films with 3%Ni:x%Co for varying cobalt concentrations (2 % and 3 %) prepared using spray pyrolysis. They observed that the electrical resistivity (ρ) decreased, reaching a minimum value on the order of 1.48×10^{-2} Ω cm for the ZnO:3%Ni:3%Co thin film. It is well known that the method of film deposition, along with the precursors and solvents utilized in the process, can influence the optoelectronic properties of the films. There exist various physical and chemical deposition techniques, with pneumatic spray pyrolysis being one of them. This method is known for its simplicity, cost-effectiveness, and the requirement of basic chemicals [18], which is why it was employed in the current study.

In this study, we examine the impact of Sn doping and (Sn, Co) co-doping on the structural, morphological, optical, and electrical properties of pure ZnO thin films. Additionally, we illustrate how this co-doping enhances the merit factor of ZnO films. The findings from this research contribute to the potential applications of the synthesized thin films in optoelectronic devices, particularly as transparent electrodes.

2. Experimental procedure

2.1. Preparation of solutions and deposition thin films

The samples used in this study were sprayed onto ordinary glass substrates using the pneumatic spray pyrolysis technique. Before each deposition, the glass substrates were carefully cleaned with acetone, followed by ethanol and finally distilled water for 15 min for each step. Then, the substrates were placed in boxes and allowed to air dry. The sources used in this work were zinc acetate dihydrate $[(CH_3COO)_2Zn{\cdot}2H_2O]$ for zinc, tin chloride $[SnCl_2]$ for tin, cobalt nitrate hexahydrate $[Co(NO_3)_2{\cdot}6H_2O]$ for cobalt, and methanol $[CH_3OH]$. A few drops of acetic acid were added to prevent the formation of zinc hydroxide. The resulting mixture was stirred at room temperature for 1 h using a magnetic stirrer to prepare a solution equal to 0.1 M. The doping contents of Sn and Co for our samples were selected as follows: (0 wt% Sn:0 wt% Co), (1 wt% Sn:0 wt% Co), (1 wt% Sn:0.5 wt% Co) and (1 wt% Sn:1 wt% Co). The pneumatic spray pyrolysis chemical deposition technique is characterized by a simple experimental setup, as illustrated in Fig. 1.

After preparing the substrates and solutions, the deposition procedure consists of several steps. Firstly, we start by turning on the hood (to evacuate the released gases), and the well-cleaned substrates are placed on the substrate holder. The entire setup is connected to an electrical resistor that serves as a temperature regulator (as shown in Fig. 1). To avoid thermal shock that could potentially damage the substrates, the substrate holder is slowly heated from room temperature to the deposition temperature, which is set at 450 °C. Subsequently, the experiment is conducted under an air pressure of 1 mbar, with the solution flow rate from the syringe pump set at 4 ml/min through a nozzle positioned 20 cm above the substrate. The values of each deposition parameter are carefully selected after numerous tests, in order to produce a high quality film suitable for an optoelectronic application. Small droplets are sprayed onto the heated substrates. The temperature effect activates the chemical reaction forming the layer while the other elements vaporize after the reaction. At the end of the deposition process, heating is stopped, and the substrates are allowed to cool slowly above the substrate holder to room temperature to avoid thermal shock. Then, the samples will be ready for various characterizations.

2.2. Testing and characterization

Each deposited thin film was characterized using various techniques for their crystalline structure using a diffractometer (PANALYTICAL Empyrean X-ray), which used CuKα radiation with a wavelength of 0.15406 nm. The Raman spectrum was obtained using a spectrometer (HORIBA LabRAM HR Evolution) at room temperature with a monochromatic radiation source emitting at a wavelength of 473 nm. The

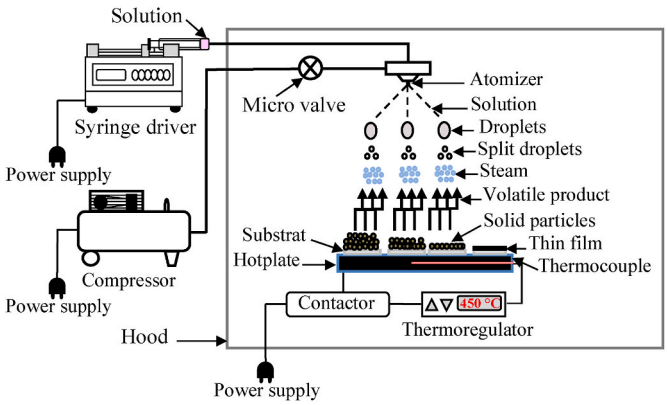

Fig. 1. Schematic diagram of the pneumatic spray technique.

measurement of the thickness of our films is done using a DECTAK3 type profilometer. Field Emission Gun Scanning Electron Microscope (FEG-SEM, JEOL FEG JSM-7100F) equipped with an elemental analysis with energy dispersive X-ray analysis (EDS). Optical transmission was quantified in the wavelength range of 300–800 nm using a Shimadzu UV-3101PC UV–Vis–NIR scanning spectrophotometer. Ultimately, the Hall effect measurement system (Ecopia HMS-3000) measured electrical properties, including carrier density, mobility, and electrical resistivity.

3. Result and discussion

3.1. Structural properties

3.1.1. X-ray diffraction (XRD) findings

Fig. 2(a) displays the XRD pattern of undoped ZnO and (Sn–Co) co-doped ZnO thin films, providing evidence for the presence of poly-crystalline ZnO in a hexagonal wurtzite phase as indicated by the standard JCPDS card n∘ 36–1451 [5]. Several authors have reported this preferential orientation [6,17–20]. This is because the plan (002) necessitates a lower amount of energy for its formation [6,20,21]. The ZnO phase purity is confirmed by the absence of peaks corresponding to Sn, Co, or their compounds in the XRD spectra. Furthermore, doping with Sn and co-doping with (Sn–Co) do not alter the preferential orientation (002), indicating that the dopants are integrated into the ZnO lattice structures. Analysis of the X-ray diffraction (XRD) patterns of the (1 % Sn)–ZnO and (1 % Sn, 0.5 % Co) co-doped ZnO films indicates that the (002) crystallographic orientation exhibits the highest intensity. This increase suggests an enhancement in the crystallinity of the ZnO films, likely due to a more controlled growth of the material and a more ordered arrangement of zinc and oxygen atoms in its crystal structure. Simultaneously, the decrease in intensity observed for doping (with 1 % Sn and 1 % Co) can be attributed to the distortions induced in the crystal structure. These phenomenon occurs due to the increase in the density of nucleation centers due to the incorporation of dopants or the increase in the degree of crystallinity, leading to grain growth with a preferred orientation along the (002) plane [22].

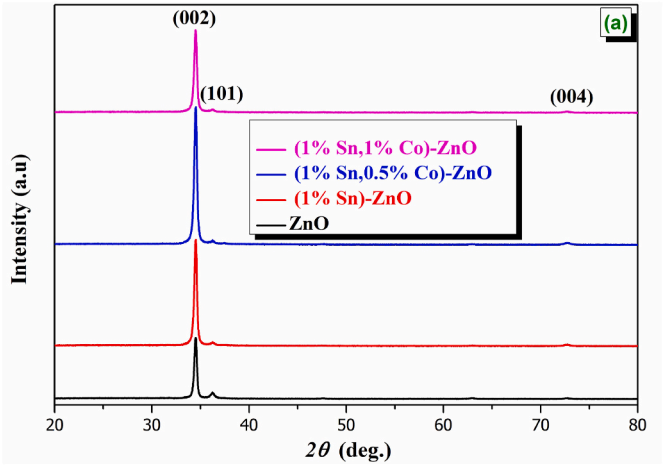

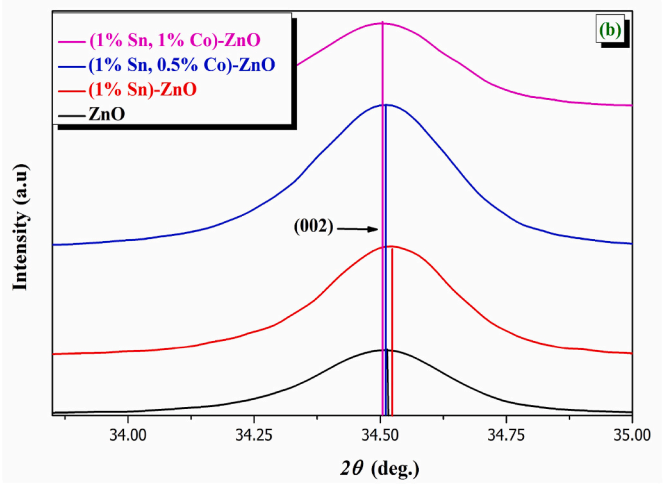

Fig. 2. (a) XRD patterns of pure ZnO and (Sn, Co)–ZnO films with different Co contents, (b) Zoom of (002) Peak positions and intensities of X-ray diffraction of obtained films.

The lattice parameter, c, has been found using the d-spacing equation for the hexagonal structure, which reduces to $c = \frac{\lambda}{\sin\theta(002)}$ for the (002) plane.

The stress (σ) in the films has been estimated by the equation [19]:

$$\sigma = \frac{-233(c - c_0)}{c_0} \quad (1)$$

Where $c_0 = 0.52066$ nm is the unstrained lattice constant for bulk ZnO, and σ is in GPa. Comparing the lattice parameter, c, values of the undoped, doped, and co-doped ZnO films listed in Table 1, it is apparent that all films exhibit a decrease in the c value. This reduction indicates the presence of tensile stresses in all films (Table 1). On the other hand, we observe a slight change in the values of parameter c. This behavior could be attributed to the difference in the ionic radii of zinc, tin, and cobalt, which are respectively 0.074, 0.069 and 0.058 nm. This result is consistent with the study by Aslan et al. [23].

Fig. 2(b) presents a zoom of XRD spectra at (002) diffraction peak region for 2θ close to 33.85°–35°. The (002) peak position and lattice constant, c, are detailed in Table 1. It is noted that the inclusion of tin (Sn) results in a minor shift of the peak towards higher 2θ values. Many researchers who have studied tin-doped ZnO at low concentrations have noted this peak shift [19,21]. This slight shift towards higher angles can be explained by the fact that the ionic radius of the Sn^{+4} dopant (0.069 nm) is smaller than that of Zn^{+2} (0.074 nm). When Sn^{+4} replaces Zn atoms in the ZnO crystal structure, this can cause compression of the surrounding chemical bonds, thereby inducing stress in (σ) the crystal structure (see Table 1). Furthermore, when the ionic radius of Sn is smaller than that of Zn, it can be relatively easily incorporated into the structure without significantly disrupting the deformations. This can result in stresses without major changes in the overall structural deformations. However, when incorporating Co, we observe a shift towards lower angles and a decrease in stresses, even though the ionic radius of Co^{+2} (0.058 nm) is smaller than that of zinc (0.074 nm). This displacement leads to a deformation of the crystal structure. Indeed, dopant ions can occupy the crystallographic sites intended for Zn ions, but because of their smaller size, they may not entirely fill the space, causing local compression and deformations in the structure. Yildirim et al. [20] and Benaicha et al. [24] have observed a comparable displacement, which they attribute to impurities as interstitial atoms within the ZnO lattice.

The crystallite size, D, lattice strain (ε) and dislocation density (δ) were estimated using the equations [6]:

$$D = \frac{0.9\lambda}{\beta \cos\theta} \quad (2)$$

$$\varepsilon = \frac{\beta}{4 \tan\theta} \quad (3)$$

$$\delta = \frac{1}{D^2} \quad (4)$$

These calculations were based on the values of β (full width at half maximum in radian), λ (wavelength of CuK radiation, 0.15406 nm), θ (angle of diffraction wavelength). Table 1 provides a summary of the calculated structural parameters. The results indicate that the ZnO film

Table 1
Structural parameters of pure, doped and co-doped ZnO films.

Samples	(002) peak position, 2θ (°)	Lattice parameter, c (nm)	FWHM, β (°)	Crystallite size, D (nm)	Strain, ε (10^{-3})	stress, σ (GPa)	Dislocation density, δ (10^{-3} nm^{-2})
ZnO	34.5161	0.51999	0.29119	31.5	4.08	0.2980	1.0078
(1%Sn)–ZnO	34.5178	0.51998	0.28706	32.1	4.00	0.3016	0.9705
(1%Sn, 0.5%Co)–ZnO	34.5089	0.52001	0.31157	29.2	4.37	0.2900	1.1728
(1%Sn, 1%Co)–ZnO	34.5020	0.52009	0.31261	29.1	4.39	0.2533	1.1809

doped with 1 % Sn exhibited an increase in crystallite size from 31.5 nm to 32.1 nm. Similar behavior has been observed in Sn-doped ZnO films by other researchers [15,25]. This increase in D suggests that Sn doping may enhance grain growth and reduce strain (Table 1). Furthermore, the crystallite size decreased to 29.2 nm and 29.1 nm, respectively, after co-doping with Co, which is in line with the findings of Caglar [26]. This reduction can be attributed to the density of nucleation centers produced by the presence of cobalt [6]. However, (Sn/Co) co-doping significantly increased dislocations (Table 1), likely due to cobalt ions potentially occupying interstitial sites. Additionally, certain co-dopants segregated within the grain boundaries [7].

3.1.2. *Raman spectroscopy findings*

The expression for the Brillouin zone center of optical phonons in the ZnO wurtzite structure is: $\Gamma_{opt} = A_1 + E_1 + 2E_2 + 2B_1$. ZnO has Raman-active E_2 nonpolar modes. The E_2 (low) mode, associated with the zinc sub-lattice, is responsive to crystal stress. On the other hand, the E_2 (high) mode is linked to the oxygen sub-lattice and is sensitive to structural damage and the creation of defects. The B_1 is silent mode. The A_1 (LO) mode is a polar Raman active mode permitted from the c face. It is highly sensitive to impurities and defects. On the other hand, the E_1 mode is polarized in the xy plane [27,28].

Fig. 3 displays the Raman spectra of undoped and (Sn–Co) co-doped ZnO thin films, within the 70–800 cm^{-1} range. The Raman spectrum of the undoped ZnO thin film displays vibration modes at 94 cm^{-1}, 432 cm^{-1} and 554 cm^{-1}, corresponding to E_2 (low), E_2 (high) and A_1 (LO). These significant Raman modes serve as confirmation of the polycrystalline nature of the ZnO thin films, indicating a hexagonal structure [29]. Additionally, the Raman spectra of the ZnO doped with Sn ions exhibit two additional peaks at 223 and 274 cm^{-1}, identified as the $2E_2$ (weak) and B_1 modes. These peaks indicate the presence of Sn ions in our structure [30]. The activation of the B_1 silent mode may be attributed to the disruption of translational crystal symmetry caused by defects, impurities, or local electric fields at grain boundaries [31]. These supplementary peaks signify the existence of secondary phases that XRD did not identify due to the detection limit [32]. We concentrate on the characteristics of the E_2 (high) mode, the A_1 (LO) mode, and their relationship for a quantitative examination of width and intensity. Fig. 4 shows the intensity ratio between A_1 (low) and E_2 (high) of the undoped, Sn-doped and (Sn, Co) co-doped ZnO thin films, According to Fig. 4, there is a noticeable rise in the ratio I (A_1 (LO))/I (E_2 (high)) for the (1% Sn)–ZnO and (1%Sn, 0.5%Co)–ZnO films. This increase could be attributed to the increase in oxygen vacancies in the crystal lattice. Oxygen vacancies have the potential to disrupt local crystal symmetry and alter electron-phonon interactions, which can lead to changes in the relative intensities of the A_1 (LO) and E_2 (high) Raman modes. However, in the case of the ZnO film co-doped with 1 % Sn and 1 % Co ((1%Sn, 1% Co)–ZnO), the ratio decreases. This reduction can be explained by the compensation effects resulting from the equality of concentrations between the dopants. When the concentrations of Sn and Co are equal, the defects introduced by these two dopants can interact and compensate each other. For example, Co ions, which act as acceptors, can neutralize donor defects introduced by Sn ions. This neutralization of defects can result in a reduction in the overall density of defects in the material. As a result, the electron-phonon interactions associated with Raman modes A_1 (LO) and E_2 (high) can be less influenced in the presence of lower defect density, leading to a decrease in the intensity ratio between these modes in the Raman spectrum. This result is in good agreement with the intensity of the (002) peak in the X-ray diffraction (XRD) spectra (Fig. 1).

3.2. *Morphological properties*

Fig. 5 displays representative FESEM images of the films cultivated on glass substrates, magnified to a scale of 70.000 times. All photos exhibit compact, homogeneous, and dense films, indicating a high-

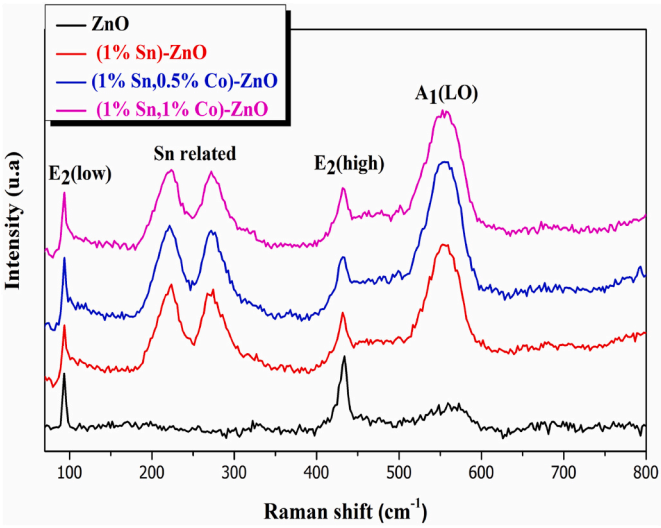

Fig. 3. Raman spectra of the undoped and (Sn, Co) co-doped ZnO thin films.

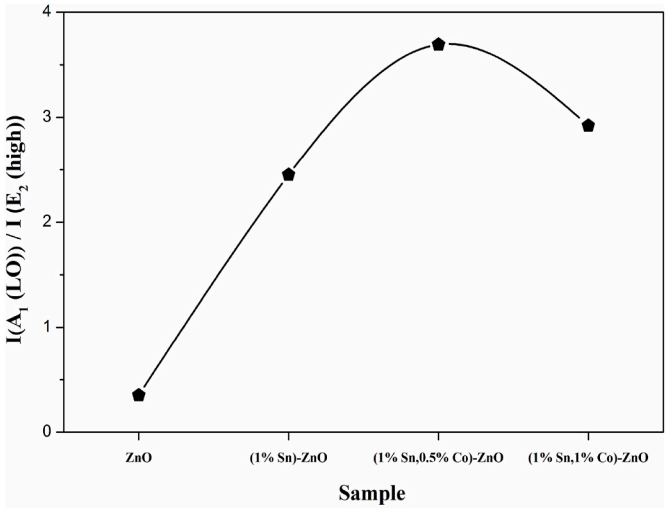

Fig. 4. The intensity ratio between A_1 (low) and E_2 (high) of the undoped, Sn-doped and (Sn, Co) co-doped ZnO thin films.

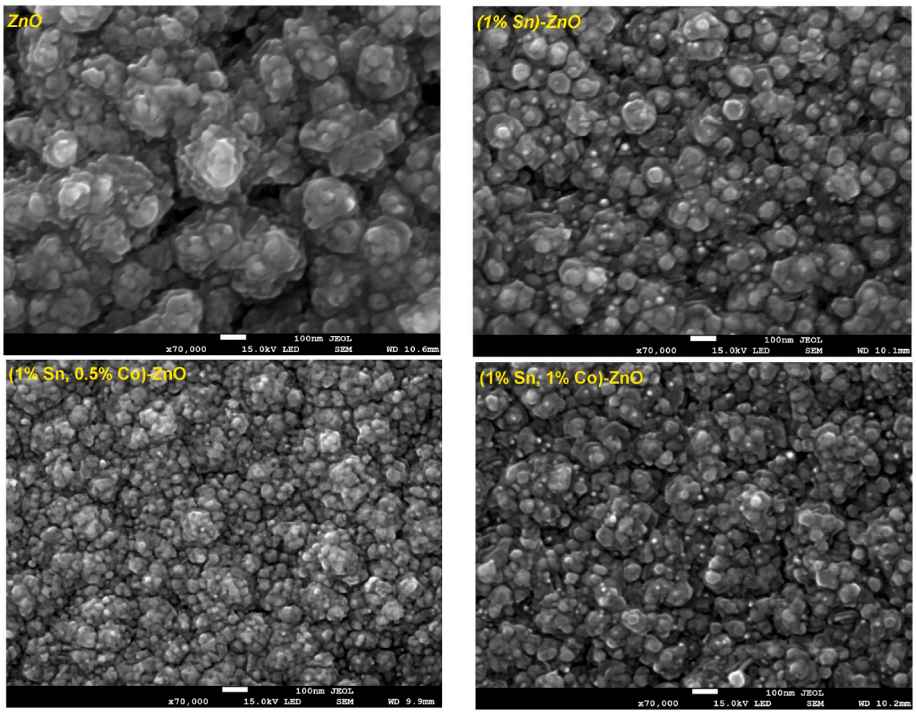

Fig. 5. Surface morphology images of the ZnO films.

quality microstructure. The micrographs demonstrate that pure and doped-ZnO films are composed of uniformly dispersed spherical nano-size grains, exhibiting a polycrystalline and continuous structure with varying forms. The kind and concentration of the dopants significantly influenced the surface morphology of the films. The particles in the ZnO thin film exhibit uneven growth patterns and form huge agglomerates. Furthermore, a small number of pits and voids are readily discernible. Upon doping with Sn, particles exhibit a more uniform and identical morphology, with a smaller size compared to the undoped ZnO particles. However, a tightly packed spherical arrangement was found in the co-doped films, resulting in a more uniform, condensed, and compact surface with smaller grains. Nevertheless, a certain quantity of atoms can be observed to be concentrated at specific grain boundaries within the Sn:Co (1 %:0.5 %) co-doped ZnO thin film. (1%Sn, 1%Co)–ZnO thin film makes this phenomenon more noticeable, which can be attributed to an increase in the concentration of Co atoms in interstitial positions, resulting in their segregation on the surface and at grain boundaries. These findings indicate a decline in the microstructural integrity of the

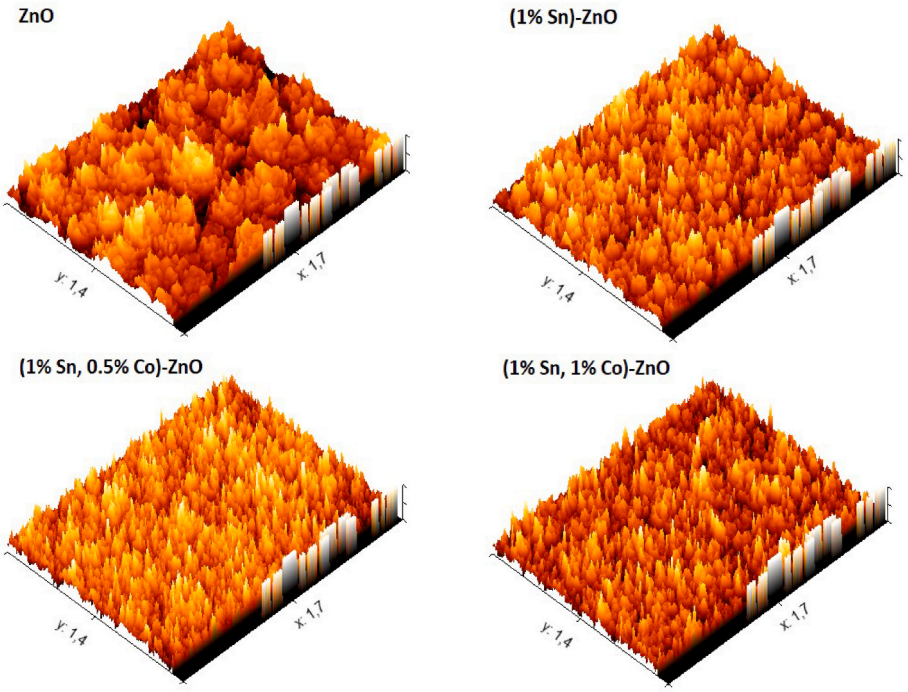

Fig. 6. 3D view of FESEM images of pure ZnO, Sn–ZnO and (Sn, Co)–ZnO films.

(1 % Sn, 1 % Co)–ZnO sample. An analogous pattern was noted for films of ZnO doped with Mg [33].

Fig. 6 displays three-dimensional representations of FESEM images depicting undoped, doped (Sn:Co) co-doped ZnO thin films. The films exhibit a columnar nanostructure that is oriented along the c-axis. An enhancement in the c-axis orientation is found for (1%Sn)–ZnO and (1% Sn, 0.5%Co)–ZnO, followed by a decrease in (1%Sn, 1%Co)–ZnO. The XRD results strongly corroborate these observations, indicating that the films demonstrate a preferential alignment along the (002) plane. The reduction in grain size of columnar crystals in the (1 % Sn, 1 % Co)–ZnO film indicates the inhibitory effect of Sn and Co co-doping on ZnO grain growth.

EDS analyses are useful for identifying the chemical purity and stoichiometry of substances. The EDS spectra of elaborated films are depicted in Fig. 7. The data unequivocally show that the pure ZnO thin film contains Zn and O elements. The incorporation of Sn and Co into ZnO is deemed successful. The weight percentages of the Sn/Zn ratio and Co/Zn ratio closely matched those of the source solution and fell within the margin of experimental error. The glass substrate is responsible for the silicon's presence in every sample. The acquired EDS data validates the prior XRD study.

3.3. Optical properties

Fig. 8 illustrates the optical transmittance spectra within the 400–800 nm wavelength range. We observe that the average transparency in the visible spectrum is approximately 74 %. All layers exhibit significant oscillations in the visible range, which are caused by the interference phenomenon resulting from the layer thickness (Table 2). This indicates that the film surface is uniform and exhibits specular properties [8], consistent with the findings from FESEM images.

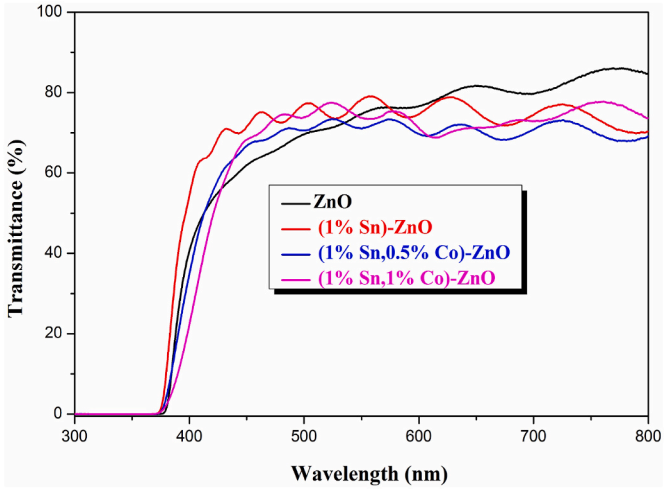

Fig. 8. Optical transmission spectra of pure ZnO, Sn–ZnO and (Sn, Co)–ZnO films.

Table 2
Values and thicknesses of prepared films.

Sample	Urbach energy, E_U (meV)	Thickness, (nm)
ZnO	327	803
(1%Sn)–ZnO	325	790
(1%Sn, 0.5%Co)–ZnO	337	828
(1%Sn, 1%Co)–ZnO	348	839

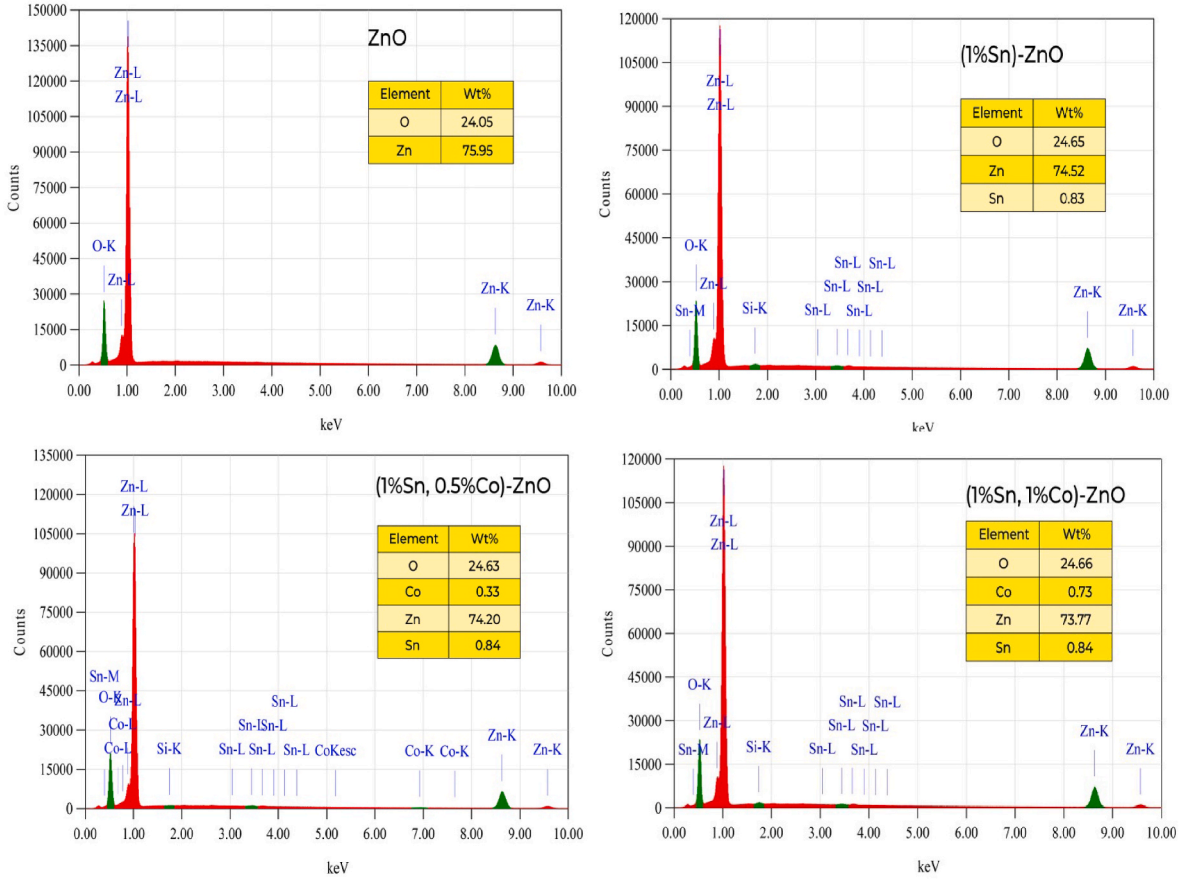

Fig. 7. Energy dispersive X-ray (EDS) spectra of pure ZnO, Sn–ZnO and (Sn, Co)–ZnO thin films.

Additionally, the average transmittance of (1%Sn)–ZnO and (1%Sn, 0.5%Co)–ZnO films falls and reaches a minimum value of 71 %, lower than that of undoped ZnO films. Then, it increases to 73 % for (1 % Sn, 0.5 % Co)–ZnO. This decrease is caused by increased defect density and oxygen deficiency from doping [17]. Additionally, the decrease in transmittance can be attributed to the higher concentrations of carriers in the lattices, which leads to enhanced scattering of photons [34]. This trend aligns well with the electrical properties, as demonstrated in the electrical results.

The optical bandgap is a important parameter for doped and co-doped films in various optical applications. ZnO is recognized as a direct bandgap semiconductor. Therefore, the optical bandgap of the films can be estimated using the Tauc relation [35]:

$$(\alpha h\nu)^2 = B\left(h\nu - E_g\right) \quad (5)$$

Which consists of the photon energy (hν), absorption coefficient (α), a constant (B), and the optical band gap (Eg). To determine the direct band gap, the linear segment of the Tauc plots is extended until it intersects with the photon energy axis, as illustrated in Fig. 9. The band gap values exhibited variation within the 3.25–3.30 eV range in response to changes in doping and co-doping concentrations. The observed higher bandgap values may be related to the Burstein-Moss effect. This phenomenon is due to the increase in the concentration of free electrons resulting from doping and co-doping [9]. Furthermore, the decrease in the density of electronic states available in the material leads to an increase in the optical gap. This can result from the formation of prohibited energy levels or from the alteration of the dispersion of electronic bands. Additionally, this increase in the optical gap for Sn:Co (1 %:0.5 %) co-doped ZnO film is attributed to the reduction in the crystallite size (Table 1). When the electrons in a semiconductor are confined to a smaller space, it results in an increase in quantum confinement energy. This is because the energy levels of the electrons become discrete, increasing the energy required to excite the electrons to higher energy levels. Moreover, the equal concentration of doping between tin (Sn) and cobalt (Co) also leads to a reduction in the optical bandgap. This reduction may be associated with the optical bandgap value of cobalt oxide (Co_3O_4), which is 1.5 eV. Additionally, the variation in the optical band gap is influenced by the intensity ratio between the A_1 (LO) and E_2 (high) modes, as shown in Fig. 4.

Urbach tail energy (E_U) measures the film network's disorder. The value of E_U was derived from the slope of the ln (αhν) plot against photon energy (Fig. 10) using the expression [21].

$$\alpha = \alpha_0 \exp\left(\frac{h\nu}{E_u}\right) \quad (6)$$

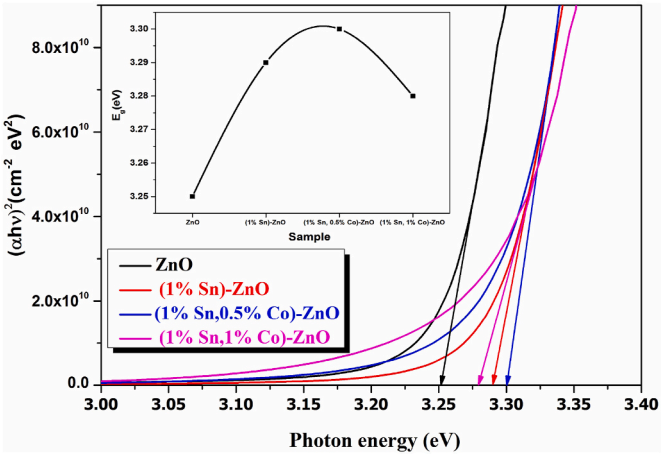

Fig. 9. The $(\alpha h\upsilon)^2$ versus hυ curves of pure ZnO, Sn–ZnO and (Sn, Co)–ZnO films. Inset shows the optical band gap as a function of (Sn and/or Co) doping.

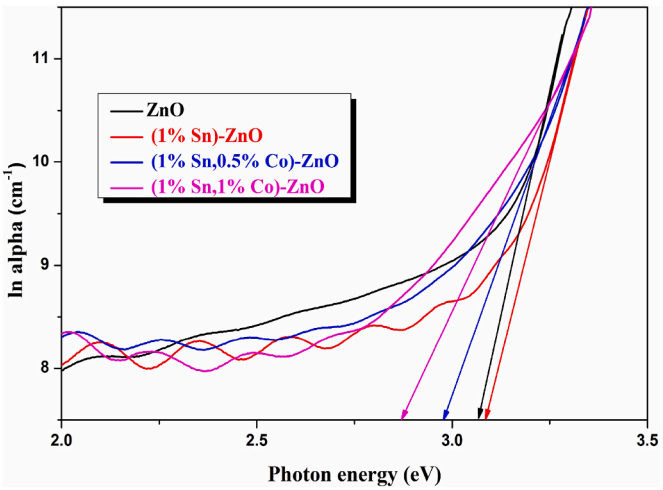

Fig. 10. Plots showing ln(α) in relation to photon energy of our films.

Where α_0 represents a constant, h denotes Planck's constant, ν is the frequency, and E_U refers to Urbach energy.

According to the information provided in Table 2, there is a similar trend between the Urbach energy and the film thickness. The incorporation of Sn into ZnO leads to a decrease in the E_U compared to undoped ZnO, likely due to a reduction in strain as indicated in Table 1. On the other hand, for the co-doped ZnO films (1%Sn, 0.5 % Co) and (1%Sn, 1% Co), there is an increase in the Urbach energy. This behavior is probably attributed to the increased thickness and insufficient time for the tin and cobalt atoms to reorganize and occupy stable sites, resulting in increased strain.

3.4. Electrical properties

Our thin films' electrical characteristics were examined using the Hall effect via van der Pauw's technique. The electrical resistivity (ρ), carrier concentration (n), and Hall mobility (μ) were determined at room temperature and are shown in Fig. 11. All films are of the n-type. The ρ initially decreases significantly from 4.87×10^{-1} Ω cm for undoped ZnO to 3.18×10^{-2} Ω cm for (1%Sn)–ZnO. This result is consistent with the findings of Tiwari et al. [11] and Serrao et al. [21], who observed a higher electrical conductivity of 7.13×10^{-1} $(\Omega\ cm)^{-1}$ and a minimum resistivity of 7.50×10^{-2} Ω cm for a ZnO film doped with 1 at.%Sn deposited by spin coating and sol-gel techniques respectively, which are higher than the electrical resistivity of 3.18×10^{-2} Ω cm obtained in this work. This difference in resistivity is attributed to the deposition technique used in this study to fabricate the Sn-doped ZnO film, compared to the same film deposited by spin-coating and sol-gel methods. This result validates the effectiveness of using tin-doped ZnO to enhance electrical conductivity. This behavior can be attributed to the incorporation of Sn^{+4} ions into the ZnO crystal lattice, where they replace Zn^{+2} sites, introducing two additional negative charges [36]. This process ultimately enhances the electrical conductivity of the material. Continuing with the same Fig., it can be observed that the resistivity continues to decrease until reaching a minimum value of 1.95×10^{-2} Ω cm, obtained for the film (1%Sn, 0.5%Co)–ZnO. It is noteworthy that the lowest electrical resistivity value ($\rho = 1.95 \times 10^{-2}$ Ω cm) achieved in this study for the co-doping of (1%Sn, 0.5%Co) is lower than the resistivity reported by Tiwari et al. [11] for a (1 at%Sn, 1 at.% Ga)-ZnO film of ρ = 78.12 Ω cm and by Salim et al. [9] for a (1 at.%Al, 0.5 at% Sn)–ZnO film with a resistivity equal to 4.405 Ω cm. Subsequently, it increases ($\rho = 4.17 \times 10^{-2}$ Ω cm) when the concentrations of Sn and Co in the ZnO film are equal at 1 %. It is important to highlight the notable difference in resistivity values between the (1%Sn, 0.5%Co)–ZnO and (1%Sn, 1%Co)–ZnO samples (Fig. 11). Many authors have reported the

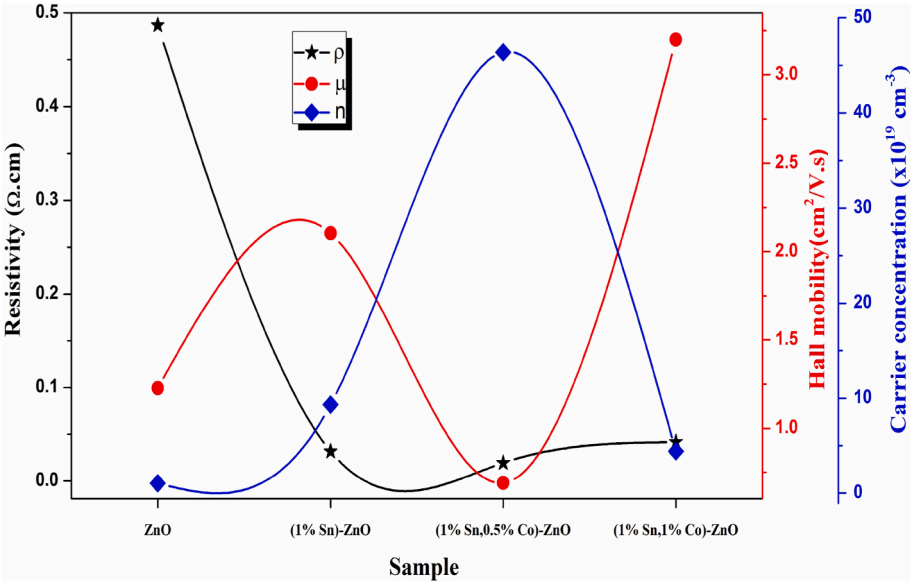

Fig. 11. Variation of resistivity (ρ), Hall mobility (μ), and carrier concentration (n) of pure ZnO, Sn–ZnO and (%Sn, %Co)–ZnO films.

same behavior in co-doped ZnO thin films [9,11]. Therefore, we can conclude that the addition of a small concentration of 0.5 % cobalt improves the electrical conductivity of the (1%Sn, x%Co)–ZnO film produced by pneumatic spray pyrolysis. This indicates that increasing the concentration of Co has a significant effect on the electrical properties and the optical gap. Moreover, the carrier concentration of the Sn–Co co-doped samples showed a significant improvement, reaching a value of 4.63×10^{20} cm^{-3} for the (1%Sn, 0.5%Co)–ZnO sample, which could explain the decrease in resistivity. Two main factors can explain the increase in the carrier concentration of the films. First, the cations (Sn^{+4}, Co^{+3}) act as donors and are incorporated into the substitutional or interstitial sites of Zn^{+2}. This increases free electrons, which contribute to electrical conduction [7]. Furthermore, there is an increase in the generation of additional oxygen vacancies (V_o) [37], particularly in the case of (1 % Sn, 0.5 % Co)–ZnO (previously reported in the Raman investigation). These oxygen vacancies function as donors in the system and acquire a positive charge, thereby releasing electrons into the conduction band [7]. In the (1%Sn, 1%Co)–ZnO thin film, the resistivity increases once more. A comparable result was reported by Lee et al. [37] for ZnO thin films co-doped with 1 at.% Sn and 1 at.% Al, elaborated using the sol-gel dip-coating technique. This increase can be attributed to a decrease in carrier concentration, which can be explained by the presence of carrier trapping sites at grain boundaries, along with a slight reduction in oxygen vacancy (V_o) defects [9,38]. Moreover, at elevated concentrations of Co, the interactions between Co and Sn atoms may alter, potentially leading to a reduction in the solubility of Co. This change could result in an increase in resistivity.

Another important parameter for evaluating the performance and quality of transparent conducting oxides (TCOs) is the Figure of Merit (FOM). Assessing the FOM provides deeper understanding of the performance and quality of the films doped with Sn and co-doped with (Sn, Co). To gauge the quality of our films and their suitability for optoelectronic applications, it is crucial to calculate the FOM using the equation [21]:

$$FOM = \frac{T^{10}}{R_s} \tag{8}$$

Where T represents the average transmittance in the wavelength range of 711–770 nm, and R_s represent the sheet resistance of the film. Fig. 12 illustrates the FOM values of various films, where a higher value indicates better film quality. The FOM values obtained for our films

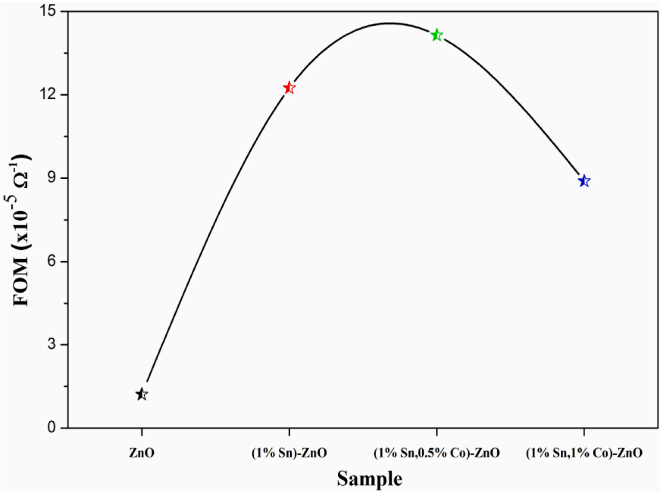

Fig. 12. Variation of the figure of merit for pure ZnO, Sn-doped ZnO and (Sn, Co)–ZnO films.

indicate an increase after doping with Sn and co-doping with (1%Sn, 0.5%Co)–ZnO, followed by a reduced variation for the (1%Sn, 1%Co)–ZnO film. In Fig. 12, the ZnO film co-doped with (1%Sn, 0.5%Co) exhibits the highest FOM value of 1.41×10^{-4} Ω^{-1}, attributed to its low electrical resistivity. Consequently, the optoelectronic quality of the deposited 0.5 % Co co-doped film is consistently enhanced.

Table 3
Deposition method, doping concentration and FOM values of reported ZnO thin films prepared by various techniques.

Samples	Deposition method	FOM, (Ω^{-1})	Ref.
3 at.%Sn–ZnO	Dip coating	5×10^{-6}	[8]
2 at.%Sn–ZnO	Spin-coating	8×10^{-9}	[21]
10 at.%Sn–ZnO	Pulsed laser deposited	7×10^{-6}	[39]
1 % Sn–ZnO	Pneumatic spray pyrolysis	1.22×10^{-4}	This work
(10 at.%F, 10 at.%Sn)–ZnO	Pulsed laser deposited	0.13×10^{-4}	[39]
(1%Sn, 0.5%Co)–ZnO	Pneumatic spray pyrolysis	1.41×10^{-4}	This work

In Table 3, we have regrouped the available data regarding the figure of merit for doped and co-doped ZnO films prepared using different methods. According to the table data, we find that the FOM value of $4 \times 10^{-4}\ \Omega^{-1}$ obtained in this study for the (1%Sn, 0.5%Co)–ZnO film is the highest among those reported.

4. Conclusion

In this study, pure, Sn-doped and (Sn/Co) co-doped ZnO thin films were produced on plain glass substrates by the pneumatic spray pyrolysis technique. The tin (Sn) concentration was fixed at 1 %, while the cobalt (Co) concentration ranged from 0 to 1 %, with increments of 0.5 %. Following the doping process with tin (Sn) and/or cobalt (Co), we observed modifications in the structural, optical, and electrical characteristics of the ZnO films. The X-ray diffraction (XRD) results confirm that all the synthesized films exhibit a hexagonal wurtzite structure typical of ZnO. A shift in the (002) peak position upon doping and co-doping indicates the incorporation of dopant ions into the ZnO lattice. The crystallite size of the film exhibited an increase with the addition of tin (Sn) doping and a decrease with co-doping. The Raman spectroscopy analysis shows an increase in the intensity ratio between the A_1 (low) and E_2 (high) modes for the (1%Sn)–ZnO and (1%Sn, 0.5%Co)–ZnO films. This increase indicates an improvement in the crystalline quality, which is consistent with the results obtained from XRD. The FESEM pictures reveal a granular structure consisting of spherical nanostructures. The incorporation of Sn and Co dopants into the ZnO matrix results in a surface that is more uniform, denser, and more cohesive, featuring finer grains.The EDS measurements confirmed the presence of Sn and Co elements in the prepared thin films. Optical measurements show that the average transparency of the films in the visible spectrum is approximately 74 %. The analysis of UV–Vis spectroscopy provide that the optical band gap for the undoped ZnO film is 3.25 eV. The widening of optical band gap from 3.23 to 3.30 eV i.e., a blue shift of absorption edge with Sn and/or Co doping is attributed to a combination of the Burstein-Moss effect and electron-impurity scattering, with a maximum value for the film (1 % Sn, 0.5 % Co)–ZnO. The analysis of Urbach energy values suggests that the introduction of tin (Sn) and cobalt (Co) dopants into the ZnO matrix increases the width of the band tail, which is associated with localized states. The electrical resistivity of the film decreases upon doping and co-doping with a minimum of $1.95 \times 10^{-2}\ \Omega$ cm for the Sn:Co (1 %:0.5 %) co-doped ZnO film. To measure the quality and efficiency of the deposited films, the Figure of Merit was calculated and it was found that the film co-doped with 0.5 % of Co shows the highest value equal at $1.41 \times 10^{-4}\ \Omega^{-1}$. The improved optical gap, low electrical resistivity and high FOM of the (1%Sn, 0.5 % Co) co-doped ZnO prepared by pneumatic spray pyrolysis film make it suitable for TCOs used as conductive transparent electrode in optoelectronic applications.

CRediT authorship contribution statement

Imadeddine Bellili: Writing – review & editing, Writing – original draft, Investigation. **Mohamed Mahtali:** Writing – review & editing, Methodology. **Warda Darenfad:** Writing – review & editing, Resources, Investigation. **Noubeil Guermat:** Writing – review & editing, Methodology.

Declaration of competing interest

The authors declare that they have no known competing financial interests or personal relationships that could have appeared to influence the work reported in this paper.

Data availability

No data was used for the research described in the article.

References

[1] N. Guermat, W. Darenfad, K. Mirouh, N. Bouarissa, M. Khalfallah, A. Herbadji, Effects of zinc doping on structural, morphological, optical and electrical properties of SnO_2 thin films, Eur. Phys. J. Appl. Phys. 97 (2022) 14, https://doi.org/10.1051/epjap/2022210218.

[2] Z. Belamri, W. Darenfad, N. Guermat, Molarity dependence of solution on structural and hydrophobic properties of ZnO nanostructures, Eur. Phys. J. Appl. Phys. 99 (2024) 10, https://doi.org/10.1051/epjap/2024230146.

[3] N. Singh, V. Khullar, Experimental and theoretical investigation into effectiveness of ZnO based transparent heat mirror covers in mitigating thermal losses in volumetric absorption based solar thermal systems, Sol. Energy 253 (2023) 439–452, https://doi.org/10.1016/j.solener.2023.02.057.

[4] B. Karki, Y. Trabelsi, A. Pal, S.A. Taya, R.B. Yadav, Direct detection of dopamine using zinc oxide nanowire-based surface plasmon resonance sensor, Opt. Mater. 147 (2024) 114555, https://doi.org/10.1016/j.optmat.2023.114555.

[5] V. Shanmugam, K.S. Jeyaperumal, Investigations of visible light driven Sn and Cu doped ZnO hybrid nanoparticles for photocatalytic performance and antibacterial activity, Appl. Surf. Sci. 449 (2018) 617–630, https://doi.org/10.1016/j.apsusc.2017.11.167.

[6] N. Guermat, W. Daranfed, I. Bouchama, N. Bouarissa, Investigation of structural, morphological, optical and electrical properties of Co/Ni co-doped ZnO thin films, J. Mol. Struct. 1225 (2021) 129134, https://doi.org/10.1016/j.molstruc.2020.129134.

[7] W. Darenfad, N. Guermat, K. Mirouh, Thoughtful investigation of ZnO doped Mg and co-doped Mg/Mn, Mg/Mn/F thin films: a first study, J. Mol. Struct. 1286 (2023) 135574, https://doi.org/10.1016/j.molstruc.2023.135574.

[8] A. Yildiz, S. Uzun, N. Serin, T. Serin, Influence of grain boundaries on the figure of merit of undoped and Al, In, Sn doped ZnO thin films for photovoltaic applications, Scripta Mater. 113 (2016) 23–26, https://doi.org/10.1016/j.scriptamat.2015.10.004.

[9] K. Salim, M. Medles, A. Nakrela, R. Miloua, A. Bouzidi, R. Desfeux, Enhancement of optical and electrical properties of spray pyrolysed ZnO thin films obtained from nitrate chemical by Al-Sn co-doping, Optik 210 (2020) 164504, https://doi.org/10.1016/j.ijleo.2020.164504.

[10] W. Darenfad, N. Guermat, K. Mirouh, A comparative study on the optoelectronic performance of undoped, Mg-doped and F/Mg co-doped ZnO nanocrystalline thin films for solar cell applications, J. Nano- Electron. Phys. 13 (2021) 06016.

[11] A. Tiwari, P.P. Sahay, Sn-Ga co-doping in sol-gel derived ZnO thin films: studies of their microstructural, optical, luminescence and electrical properties, Mater. Sci. Semicond. Process. 118 (2020) 105178.

[12] S. Roguai, A. Djelloul, Sn doping effects on the structural, microstructural, Seebeck coefficient, and photocatalytic properties of ZnO thin films, Solid State Commun. 350 (2022) 114740, https://doi.org/10.1016/j.ssc.2022.114740.

[13] R. Munprom, C. Sae-tiaw, S. Phiankoh, O. Jongprateep, K. Surawathanawises, R. Techapiesancharoenkij, Structural, optical, and electrical modification of hydrothermally grown ZnO nanorods by tin-doping, Mater. Res. Express 6 (2019) 095916, https://doi.org/10.1088/2053-1591/ab349f.

[14] A. Tiwari, P.P. Sahay, Modification in the physical properties of nanocrystalline ZnO thin films by Sn/Ni co-doping for transparent conductive oxide applications, Phys. B Condens. Matter 629 (2022) 413638, https://doi.org/10.1016/j.physb.2021.413638.

[15] V. Ganesh, I.S. Yahia, S. Al Faify, M. Shkir, Sn-doped ZnO nanocrystalline thin films with enhanced linear and nonlinear optical properties for optoelectronic applications, J. Phys. Chem. Solid. 100 (2017) 115–125, https://doi.org/10.1016/j.jpcs.2016.09.022.

[16] I. Benaicha, I. Jellal, J. Mhalla, A. Fahmi, M. Addou, A. Qachaou, M. Fahoume, Atmospheric growth of ZnO thin films doped and co-doped with Ni and Co via UMVD: experimental and theoretical study, J. Mater. Sci. Mater. Electron. 33 (2022) 6999–7010, https://doi.org/10.1007/s10854-022-07880-z.

[17] B. Demirselcuk, V. Bilgin, Ultrasonically sprayed ZnO:Co thin films: growth and characterization, Appl. Surf. Sci. 273 (2013) 478–483, https://doi.org/10.1016/j.apsusc.2013.02.065.

[18] W. Darenfad, N. Guermat, N. Bouarissa, F.Z. Satour, A. Zegadi, K. Mirouh, Improvement in optoelectronics and photovoltaic properties of p-Co_3O_4/n-ZnO hetero-junction : effect of deposition time of sprayed Co_3O_4 thin films, J. Mater. Sci. Mater. Electron. 35 (162) (2024) 1–13.

[19] A. Tiwari, P.P. Sahay, Highly c-axis oriented (Mg, Sn) co-doped ZnO thin films for optoelectronic applications, Opt. Mater. 134 (2022) 13098, https://doi.org/10.1016/j.optmat.2022.113098.

[20] O.A. Yildirim, H. Arslan, S. Sönmezoğlu, Facile synthesis of cobalt-doped zinc oxide thin films for highly efficient visible light photocatalysts, Appl. Surf. Sci. 390 (2016) 111–121, https://doi.org/10.1016/j.apsusc.2016.08.069.

[21] F.J. Serrao, N.N. Bappalige, K.M. Sandeep, S. Raghavendra, Dominance of c-axis orientation on the carrier transport properties of Sn doped ZnO thin films, Thin Solid Films 722 (2021) 138579, https://doi.org/10.1016/j.tsf.2021.138579.

[22] A.M. Alsaad, A.A. Ahmad, Q.M. Al-Bataineh, A.A. Bani-Salameh, H.S. Abdullah, I. A. Qattan, Z.M. Albataineh, A.D. Telfah, Optical, structural, and crystal defects characterizations of dip synthesized (Fe-Ni) Co-doped ZnO thin films, Materials 13 (2020) 1737, https://doi.org/10.3390/ma13071737.

[23] E. Aslan, M. Zarbali, Tuning of photosensitivity and optical parameters of ZnO based photodetectors by co-Sn and Ti doping, Opt. Mater. 125 (2022) 112030, https://doi.org/10.1016/j.optmat.2022.112030.

[24] I. Benaicha, I. Jellal, J. Mhalla, A. Fahmi, M. Addou, A. Qachaou, M. Fahoume, Atmospheric growth of ZnO thin films doped and co-doped with Ni and Co via

UMVD: experimental and theoretical study, J. Mater. Sci. Mater. Electron. 33 (2022) 6999–7010, https://doi.org/10.1007/s10854-022-07880-z.
[25] M. Ajili, M. Castagné, N. Kamoun Turki, Study on the doping effect of Sn-doped ZnO thin films, Superlattice. Microst. 53 (2013) 213–222, https://doi.org/10.1016/j.spmi.2012.10.012.
[26] Y. Caglar, Sol–gel derived nanostructure undoped and cobalt doped ZnO: structural, optical and electrical studies, J. Alloys Compd. 560 (2013) 181–188, https://doi.org/10.1016/j.jallcom.2013.01.080.
[27] M. Mehedi Hassan, W. Khan, P. Mishra, S.S. Islam, A.H. Naqvi, Enhancement in alcohol vapor sensitivity of Cr doped ZnO gas sensor, Mater. Res. Bull. 93 (2017) 391–400, https://doi.org/10.1016/j.materresbull.2017.05.019.
[28] R. Vettumperumal, S. Kalyanaraman, B. Santoshkumar, R. Thangavel, Estimation of electron–phonon coupling and Urbach energy in group-I elements doped ZnO nanoparticles and thin films by sol–gel method, Mater. Res. Bull. 77 (2016) 101–110, https://doi.org/10.1016/j.materresbull.2016.01.015.
[29] Z. Belamri, W. Darenfad, N. Guermat, Impact of annealing temperature on surface reactivity of ZnO nanostructured thin films deposited on aluminum substrate, J. Nano- Electron. Phys. 15 (2023) 02026, https://doi.org/10.21272/jnep.15(2).02026.
[30] A. Bedia, F.Z. Bedia, M. Aillerie, N. Maloufi, Structural, electrical and optical properties of Al–Sn codoped ZnO transparent conducting layer deposited by spray pyrolysis technique, Superlattice. Microst. 111 (2017) 714–721, https://doi.org/10.1016/j.spmi.2017.07.031.
[31] V. Russo, M. Ghidelli, P. Gondoni, C.S. Casari, A. Li Bassi, Multi-wavelength Raman scattering of nanostructured Al-doped zinc oxide, J. Appl. Phys. 115 (2014) 073508, https://doi.org/10.1063/1.4866322.
[32] A. Mahroug, S. Boudjadar, S. Hamrit, L. Guerbous, Structural, morphological and optical properties of undoped and Co-doped ZnO thin films prepared by sol–gel process, J. Mater. Sci. Mater. Electron. 25 (2014) 4967–4974, https://doi.org/10.1007/s10854-014-2259-6.
[33] A.J. Kulandaisamy, J.R. Reddy, P. Srinivasan, K. Jayanth Babu, G. Kumar Mani, P. Shankar, J.B. Balaguru Rayappan, Room temperature ammonia sensing properties of ZnO thin films grown by spray pyrolysis: effect of Mg doping, J. Alloys Compd. 688 (2016) 422–429, https://doi.org/10.1016/j.jallcom.2016.07.050.
[34] K. Ravichandran, A. Anbazhagan, N. Dineshbabu, C. Ravidhas, Influence of Mo doping on transparent conducting properties of ZnO films prepared by a simplified spray technique, J. Mater. Sci. Mater. Electron. 26 (2015) 7649–7654, https://doi.org/10.1007/s10854-015-3404-6.
[35] N. Guermat, W. Darenfad, K. Mirouh, M. Kalfallah, M. Ghoumazi, Super-hydrophobic F-doped SnO_2 (FTO) nanoflowers deposited by spray pyrolysis process for solar cell applications, J. Nano- Electron. Phys. 15 (2022) 05013, https://doi.org/10.21272/jnep.14(5).05013.
[36] A. Phuruangrat, S. Kongnuanyai, T. Thongtem, S. Thongtem, Ultrasound-assisted synthesis, characterization and optical property of 0–3 wt% Sn-doped ZnO, Mater. Lett. 91 (2013) 179–182, https://doi.org/10.1016/j.matlet.2012.09.091.
[37] M.I. Lee, M.C. Huang, D. Legrand, G. Lerondel, J.C. Lin, Structure and characterization of Sn, Al co-doped zinc oxide thin films prepared by sol–gel dip-coating process, Thin Solid Films 570 (2014) 516–526, https://doi.org/10.1016/j.tsf.2014.04.051.
[38] S.C. Chen, C.H. Wang, H. Sun, C.K. Wen, C.F. Lu, C.L. Tsai, Y.K. Fu, T.H. Chuang, Microstructures, electrical and magnetic properties of (Ga, Co)-ZnO films by radio frequency magnetron co-sputtering, Surf. Coat. Technol. 303 (2016) 203–208, https://doi.org/10.1016/j.surfcoat.2016.03.064.
[39] A. Mallick, S. Ghosh, D. Basak, Highly conducting and transparent low-E window films with high figure of merit values based on RF sputtered Al and in co-doped ZnO, Mater, Sci. Semicond. Process. 119 (2020) 105240, https://doi.org/10.1016/j.mssp.2020.105240.